ARTICLE

Giant Electroresistance of Super-tetragonal $BiFeO_3$-Based Ferroelectric Tunnel Junctions

Hiroyuki Yamada,[†,‡] Vincent Garcia,[†,*] Stéphane Fusil,[†,§] Sören Boyn,[†] Maya Marinova,[⊥] Alexandre Gloter,[⊥] Stéphane Xavier,[||] Julie Grollier,[†] Eric Jacquet,[†] Cécile Carrétéro,[†] Cyrile Deranlot,[†] Manuel Bibes,[†] and Agnès Barthélémy[†]

[†]Unité Mixte de Physique CNRS/Thales, 1 Avenue Augustin Fresnel, Campus de Polytechnique, 91767 Palaiseau, France, and Université Paris-Sud, 91405 Orsay, France, [‡]National Institute of Advanced Industrial Science and Technology (AIST), Higashi 1-1-1, Tsukuba, Ibaraki 305-8562, Japan, [§]Université d'Evry-Val d'Essonne, Boulevard F. Mitterrand, 91025 Evry, France, [⊥]Laboratoire de Physique des Solides, Bâtiment 510, CNRS UMR 8502, Université Paris Sud XI, 91405 Orsay, France, and [||]Thales Research and Technology, 1 Avenue Augustin Fresnel, Campus de Polytechnique, 91767 Palaiseau, France

ABSTRACT Ferroelectric tunnel junctions enable a nondestructive readout of the ferroelectric state *via* a change of resistance induced by switching the ferroelectric polarization. We fabricated submicrometer solid-state ferroelectric tunnel junctions based on a recently discovered polymorph of $BiFeO_3$ with giant axial ratio ("T-phase"). Applying voltage pulses to the junctions leads to the highest resistance changes (OFF/ON ratio >10 000) ever reported with ferroelectric tunnel junctions. Along with the good retention properties, this giant effect reinforces the interest in nonvolatile memories based on ferroelectric tunnel junctions. We also show that the changes in resistance scale with the nucleation and growth of ferroelectric domains in the ultrathin $BiFeO_3$ (imaged by piezoresponse force microscopy), thereby suggesting potential as multilevel memory cells and memristors.

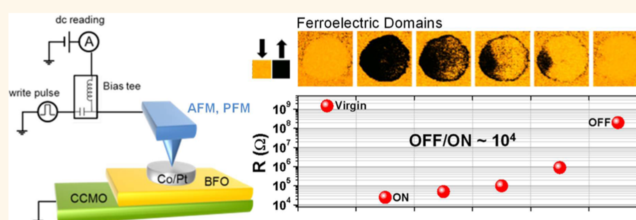

KEYWORDS: ferroelectric tunnel junctions · nanoscale ferroelectrics · tunnel electroresistance · bismuth ferrite · piezoresponse force microscopy

Ferroelectrics possess a spontaneous polarization that is switchable by applying an electric field. Thick layers of ferroelectric materials are currently commercially available as ferroelectric random access memories (FeRAMs).[1] When the thickness of the ferroelectric reaches a few nanometers, electron tunneling becomes possible.[2] In ferroelectric tunnel junctions (FTJs),[3] where such an ultrathin ferroelectric film is sandwiched between two electrodes, any asymmetry between the two metal/ferroelectric interfaces (different metals, different interface terminations, *etc.*) will give rise to an asymmetric electrostatic potential distribution caused by the ferroelectric polarization. When switching the polarization orientation, the averaged barrier height of the tunnel barrier changes, resulting in potentially large changes of the tunnel current, as it depends exponentially on the square root of the barrier height.[4,5] This large contrast called tunnel electroresistance is appealing, as it provides a simple means for the nondestructive resistive readout of the ferroelectric polarization state.[6] FTJs may thus combine the advantages of FeRAMs, such as speed, reliability, and fatigue, with the architectural simplicity and scalability of other resistive random access memories (RRAMs). Large tunnel electroresistance was first demonstrated on bare surfaces of ultrathin ferroelectrics using a conductive atomic force microscope (AFM) tip as top electrode.[6−8] More recently, several groups demonstrated tunnel electroresistance in solid-state FTJs based on $BaTiO_3$[9−13] or Pb(Zr,Ti)O_3[14,15] ultrathin films. Here we report results on FTJs based on a previously unexplored ferroelectric barrier, $BiFeO_3$.

FTJs were defined from ultrathin films of the recently discovered polymorph of $BiFeO_3$ (BFO) having a tetragonal-like structure with giant axial ratio ("T-phase" BFO). This phase is expected to have a large polarization

* Address correspondence to vincent.garcia@thalesgroup.com.

Received for review March 11, 2013 and accepted May 6, 2013.

Published online May 06, 2013
10.1021/nn401378t

© 2013 American Chemical Society

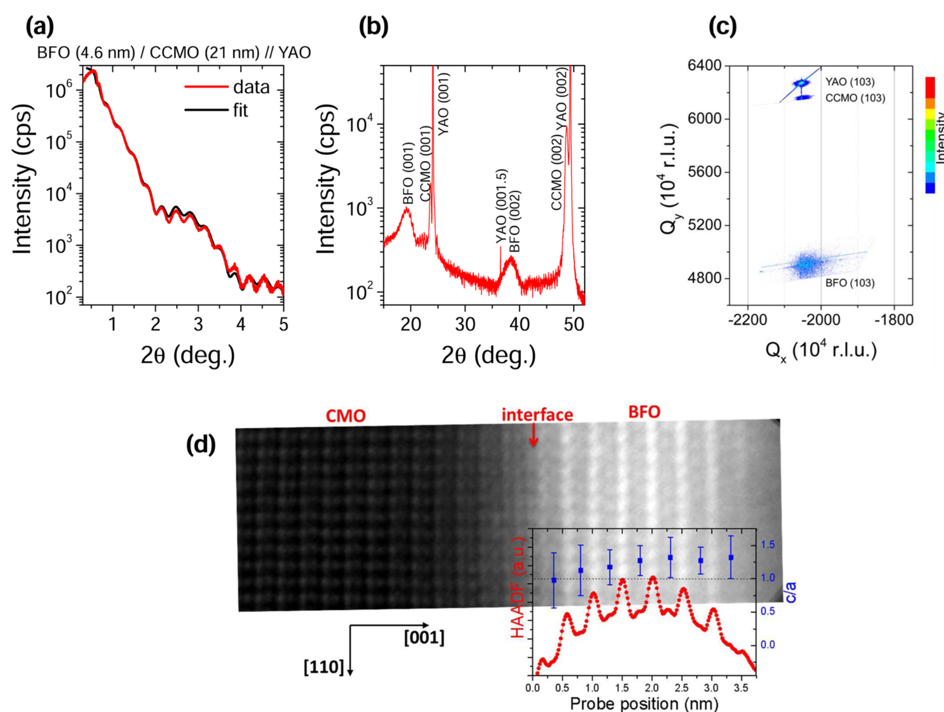

Figure 1. (a) X-ray reflectivity data of the BFO/CCMO bilayer grown on YAO substrate. The black line is the best fit obtained for BFO (4.6 nm)/CCMO (21 nm). (b) $\omega-2\theta$ X-ray diffraction pattern of the same sample showing a single-phase super-tetragonal BFO phase. The diffraction peaks are indexed in pseudocubic notation. (c) Reciprocal space mapping around YAO(103), CCMO(103), and BFO(103). (d) HAADF image of the BFO/CMO interface together with the *c*/*a* ratio within the BFO layer starting from the CMO interface.

(up to 150 μC/cm^2),[16−19] which was partially confirmed by recent experiments.[20,21] In order to stabilize this BFO phase with giant tetragonal distortion [$a \approx 0.377$ nm, $c \approx 0.465$ nm (ref 20)], ultrathin films of BFO were grown on (001)$YAlO_3$ (YAO, average in-plane parameter in pseudocubic notation $a = 0.371$ nm) substrates by pulsed laser deposition using a Nd:YAG laser. $Ca_{0.96}Ce_{0.04}MnO_3$ (CCMO) thin films, which are well lattice-matched with YAO, were used as bottom electrodes.[22] The thicknesses of BFO and CCMO layers were estimated by X-ray reflectivity to be 4.6 and 21 nm, respectively (Figure 1a). $\omega-2\theta$ X-ray diffraction scans (Figure 1b) and reciprocal space maps (Figure 1c) reveal that the BFO film is purely in its T-phase with a large out-of-plane parameter of 0.47 nm and a strained in-plane parameter of 0.37 nm. An aberration-corrected scanning transmission electron microscope (STEM), NION UltraSTEM200, equipped with a cold-field emission electron source operated at 100 kV, was used to examine cross sections of similar BFO (3.5 nm)/$CaMnO_3$ (10 nm)/$Ca_{0.96}Ce_{0.04}MnO_3$(20 nm)// YAO (001) structures. A high-angle annular dark field (HAADF) image of the BFO/CMO interface is shown in Figure 1d together with the evolution of the *c*/*a* ratio within the BFO layer. Apart from the first unit cell, the *c*/*a* ratio is 1.2, corresponding to the T-phase throughout the BFO thickness.

Solid-state FTJs with diameters ranging from 180 to 600 nm were defined by a single-step e-beam lithography process and lift-off of top Pt (10 nm)/Co (10 nm) electrodes grown by sputtering.[9] These Pt/Co/BFO/CCMO junctions were connected electrically by a conductive AFM tip to allow resistance measurements as well as piezoresponse force microscopy (PFM) imaging[23,24] after applying 100 ns write voltage pulses[25] (Figure 2b).

RESULTS AND DISCUSSION

Figure 2a shows a typical hysteresis curve of resistance *vs* write voltage pulses (V_{write}) obtained on a 180 nm wide capacitor. The device resistance is initially $(2-3) \times 10^9$ Ω in the virgin state. Applying negative voltage pulses with increasing amplitude virtually does not change the resistance state of the device until a threshold voltage of $V_{write} = -2.5$ V to -3 V (cycle 1). At this voltage, the resistance drops by 5 orders of magnitude to $(2-3) \times 10^4$ Ω (ON state). When V_{write} is then swept from -3 V to $+3$ V, the resistance is stable up to a threshold voltage of $+1.5$ V, where it starts increasing. The resistance increases more progressively when increasing V_{write} to $+3$ V and saturates around $(3-4) \times 10^8$ Ω (OFF state). When sweeping again V_{write} from $+3$ V to -3 V, the device resistance goes back to the ON state at a slightly lower threshold V_{write} of -2 V (cycle 2). It switches back to the OFF state in the same manner when V_{write} varies from -3 V to $+$ 3 V (cycle 3). The OFF/ON ratio is then typically over 10 000 within a write pulse window of ± 3 V. Importantly, intermediate resistance states can be stabilized by decreasing the maximum V_{write} to $+2.5$ V (cycle 4) or

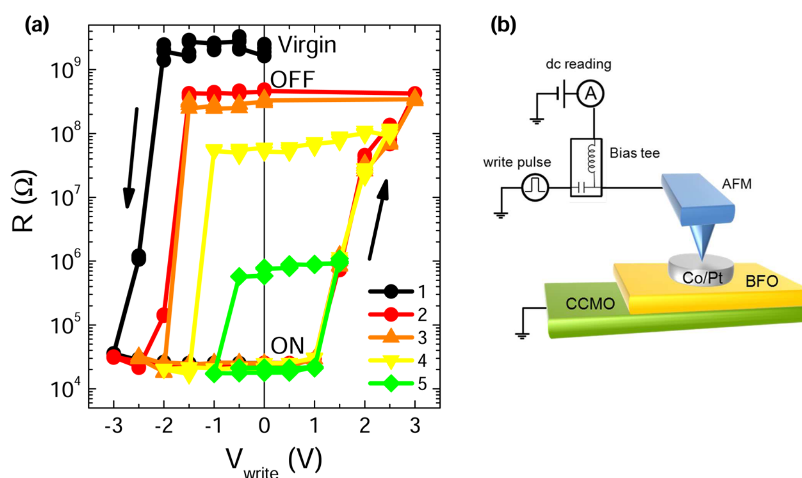

Figure 2. (a) Typical hysteresis of resistance with write voltage pulses of a 180 nm wide Pt/Co/BFO/CCMO capacitor. Cycle 1 shows the first switching from the virgin state to the ON state. Cycles 2 and 3 show reproducible hysteresis from the ON to the OFF state. Cycles 4 and 5 represent minor loops with intermediate resistance states. (b) Sketch of the experiment where the capacitor is connected *via* the AFM tip. A bias tee ensures the separation between voltage pulses to write the information and the dc circuit to read the resistance state of the device.

+1.5 V (cycle 5), so that the devices display a memristive behavior.[26,27]

To understand the resistance variations observed in Figure 2a, we used PFM to visualize the ferroelectric domain structure of BFO through the top Pt/Co electrode. Practically, we first switch the FTJ to a given resistance through the application of voltage pulses and subsequently perform PFM. Figure 3a shows the piezoresponse phase signal (top) and amplitude (bottom) of a virgin 180 nm junction with a resistance of (1–2) × 10^9 Ω (Figure 3g). The phase is completely bright and the amplitude is strong and constant on the whole junction area. This corresponds to a homogeneous polarization pointing toward CCMO (as deduced from the sign of the bias needed for ferroelectric switching). In PFM, the virgin states of all FTJs with various diameters between 180 and 600 nm are identical, with polarization pointing downward; they all are in a high resistance state with a constant resistance–area product of about (3–4) × 10^7 Ω·μm^2. After switching the 180 nm junction to the ON state ((2–3) × 10^4 Ω) with negative voltage pulses, the PFM phase homogeneously shifts by 180 degrees, except for a few regions on the right side of the device (Figure 3b). The PFM amplitude (bottom panel) is large only on the left side, consistent with a saturated state with polarization pointing up in this part of the junction. On the right side, the amplitude is lower, indicating that this half of the device is in a mixed state with incomplete switching; because the phase is globally dark, it consists of a majority of domains with upward polarization and nanodomains pinned with downward polarization. Overall, most of the BFO has a polarization pointing toward Co in the ON state. Analysis of the PFM images yields a relative fraction of down domains (hereinafter designated as *s*) of only about 1%.

When the junction resistance is slightly increased (5 × 10^4 Ω) by positive voltage pulses, bright domains

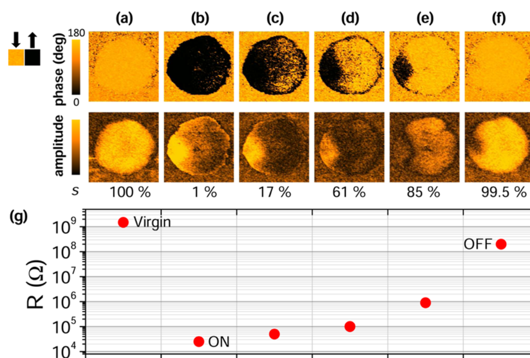

Figure 3. Piezoresponse force microscopy imaging for different resistance states of a 180 nm wide Pt/Co/BFO/CCMO capacitor. (a) Virgin state. (b) ON state. (c, d, e) Successive intermediate states with increasing resistances. (f) OFF state. Out-of-plane PFM phase (top panel) and amplitude (bottom panel) for each state. The same amplitude scale was used for all images. The estimated fraction of down domains (*s*) is noted for each state. (g) Resistance of the different states. The size of the points represents typical error bars during resistance measurements.

nucleate/propagate around the preexisting bright nanodomains on the right side (Figure 3c, top panel). Accordingly, the amplitude is strongly decreased in this mixed area (Figure 3c, bottom panel) due to the higher density of domain walls that give zero PFM amplitude. As the resistance reaches 1 × 10^5 Ω, the bright domains propagate (Figure 3d, top panel) and the amplitude starts to kick in on the right side and decreases on the left side. For a resistance of 9 × 10^5 Ω, the down domains in the right area coalesce and the phase becomes homogeneously bright (Figure 3e, top panel). On the left side, bright domains nucleate within the dark domain area. The amplitude of the two opposite domains is similar and decreases only at an intermediate region that resembles a domain wall (Figure 3e, bottom panel). In the OFF state (2 × 10^8 Ω),

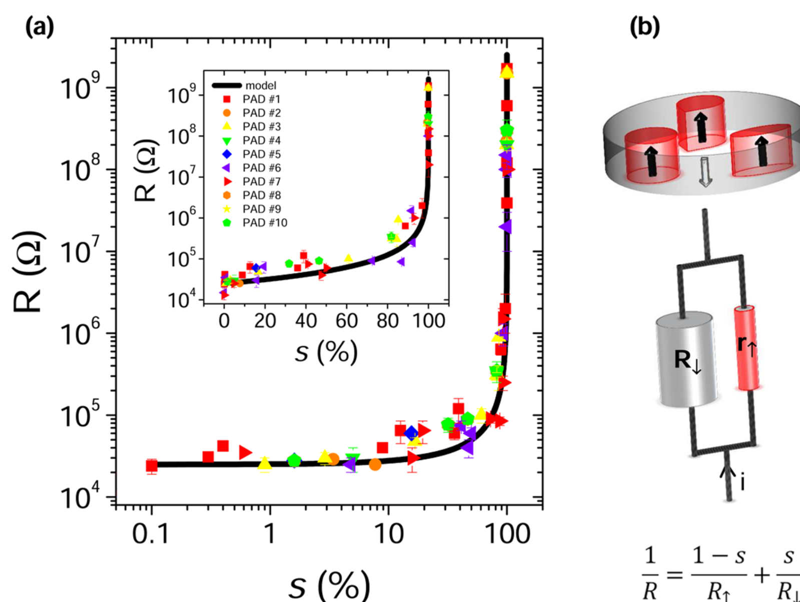

Figure 4. Scaling of the resistance state with the fraction of down domains. 100 ns pulses with variable amplitudes are applied to 10 devices with the same diameter (180 nm). The device resistance is then measured followed by a PFM image of the ferroelectric domains. (a) Device resistance as a function of the fraction of down domains in log−log scale (log−linear scale in inset). The black line is calculated using the parallel conduction model sketched in (b).

the phase is completely bright with some noise on the left area, and the amplitude is strong except for the same area of the left side (Figure 3f). These observations suggest that nanodomains (smaller than the tip radius) with upward polarization persist in the OFF state. Once created (Figure 2a, cycle 1), these pinned nanodomains with upward polarization cannot be erased and lead to a lower resistance state in the OFF state than in the virgin state. They act as nuclei and diminish the negative threshold voltage needed to switch the capacitor to the ON state in subsequent cycles (Figure 2a, cycle 2).

We investigated ten 180 nm junctions in the same way, combining PFM and electrical measurements in various resistance states. The fraction of down domains s is estimated for each PFM image. Figure 4a shows a plot of the resistance of these devices, which increases as a function of s. The results can be interpreted using a simple model where down and up ferroelectric domains conduct in parallel (Figure 4b). The black line in Figure 4a is calculated with a resistance of 2.5×10^4 Ω when the polarization points toward Co and 2.5×10^9 Ω when it points toward CCMO. The experimental data of the 10 junctions agree very well with this simple parallel conduction model. This clearly suggests that resistive switching in Co/BFO/CCMO tunnel junctions results from the nucleation and propagation of up/down ferroelectric domains. It also indicates that in ultrathin T-phase BFO films the conduction of ferroelectric domain walls[28,29] can be neglected over the tunnel conductance through the domains, although it could give second-order contributions to the resistance variations.

Retention experiments were performed on an array of four FTJs with a diameter of 180 nm. All the devices were switched to different resistance states and imaged with PFM (Figure 5a−d). Pad #1 was switched close to the ON state (Figure 5a). Pads #2 and #3 were switched to two different intermediate states (Figure 5b and c). Pad #4 was first switched to the ON state and then close to the OFF state (Figure 5d). Three days later (68 h), the same devices were imaged by PFM and measured electrically (Figure 5f−i). Note that the apparent distortion of the pads from a regular circular shape is only due to image drifts during PFM imaging, not to effective geometric changes. Figure 5f shows the PFM signal of pad #1, where small bright domains have nucleated in the bottom part of the capacitor (top panel) accompanied by a reduction of the amplitude (bottom panel). The PFM images of pads #2 (Figure 5g), #3 (Figure 5h), and #4 (Figure 5i) are very similar after three days in both phase and amplitude. Figure 5j displays the resistance level of the four devices, with relatively small resistance variations over three days. It should be noted that the large ac signal (compared to coercive thresholds) required for PFM experiments sometimes slightly destabilizes the ferroelectric domain configuration. Overall, these BFO-based FTJs thus show good retention properties, even in intermediate resistance states.

Figure 5k shows fatigue measurements over 2000 cycles on a single Co/BFO/CCMO device with a diameter of 300 nm. Each cycle consists in applying a pulse of +2.5 V, reading the resistance twice, applying a pulse of −3 V, and reading the resistance twice. The resistance contrast between the two states is 1000 all

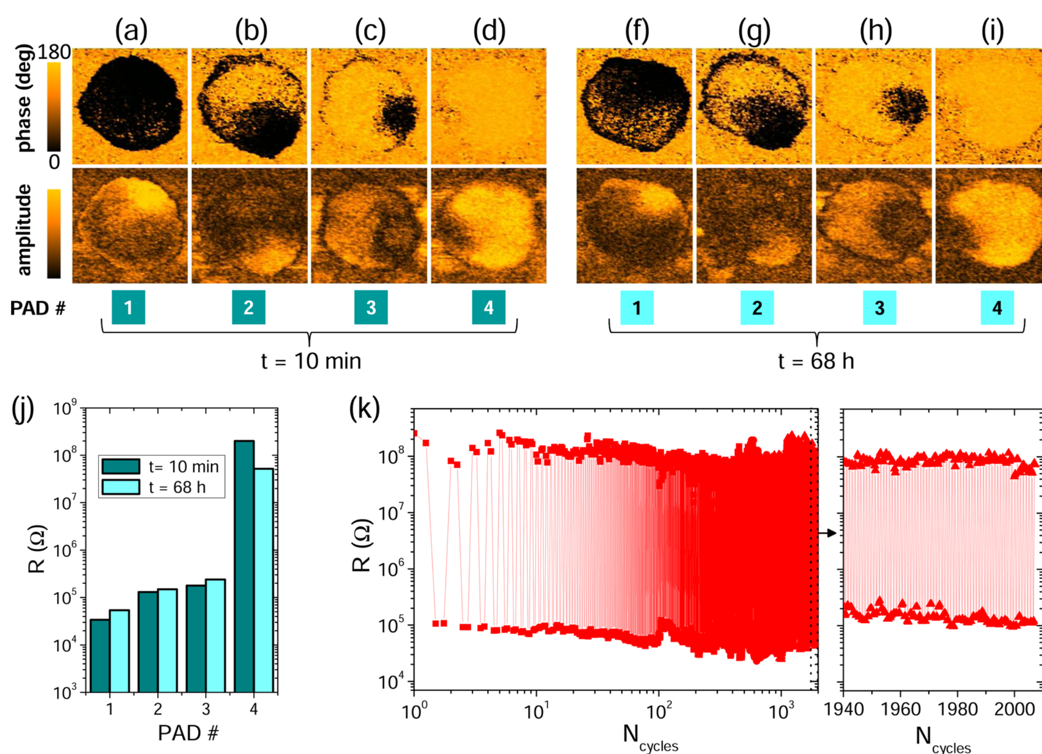

Figure 5. Retention and fatigue properties of ferroelectric tunnel junctions. (a–d) Four 180 nm wide devices are imaged with PFM in four different resistance states. (f–i) The same devices are imaged with PFM 68 h later. (j) Resistance of the four devices initially and after 68 h. (k) Fatigue on a 300 nm wide capacitor for 2000 cycles. Each cycle consists of writing at +2.5 V, reading twice, writing at −3 V, and reading twice.

along the experiment, with slight oscillations of the extreme resistance levels. This supports[9] the absence of fatigue for FTJs in endurance testing conditions based on a scanning probe setup.

CONCLUSIONS

To summarize, we demonstrated a very large OFF/ON ratio >10 000 in 180 nm wide ferroelectric tunnel junctions based on T-type BFO. PFM evidences the nucleation and propagation of domains in the ferroelectric barrier, just as was widely reported in thicker ferroelectric films.[23,24] The resistive switching is correlated to the ferroelectric switching and the resistance with the domain population within a parallel conduction model. The devices show good retention properties within three days with persistent PFM signal of the various complex ferroelectric domain configurations corresponding to the whole range of resistance levels. These results open the path to investigate the dynamics of nanoscale ferroelectrics embedded in active devices used as nonvolatile memories, as the simple measurement of the resistance state is directly correlated with the ferroelectric domain configuration.

METHODS

Sample Preparation. CCMO was grown at 670 °C under an oxygen pressure of 0.2 mbar, and BFO was subsequently grown at 580 °C with an oxygen pressure of 6×10^{-3} mbar. The samples were then annealed for 30 min at 500 °C under high oxygen pressure (300 mbar).

Piezoresponse Force Microscopy and Electrical Measurements. All the measurements were performed with a multimode Nanoscope IV (Digital Instruments) setup at room temperature and under nitrogen flow using commercial Si tips coated with Cr/Pt (Budget Sensors). The bias voltage was applied to the tip, and the sample was grounded for electrical measurements. A bias tee was connected to the atomic force microscope to split voltage pulses from dc measurements. The device resistances were measured at constant voltage (V_{DC} = −200 mV). PFM experiments were conducted with SR830 lock-in detection. For PFM imaging, a TTi TG1010 external source was used to apply a 14 kHz ac sinusoidal excitation of 600 mV peak to peak with a dc offset of 200 mV. The tip was grounded for PFM experiments.

Conflict of Interest: The authors declare no competing financial interest.

Acknowledgment. The authors acknowledge financial support from the European Research Council (ERC Advanced Grant FEMMES, No. 267579) and the French Agence Nationale de la Recherche (ANR) through projects MHANN, NOMILOPS, and MULTIDOLLS.

REFERENCES AND NOTES

1. Scott, J. F. Applications of Modern Ferroelectrics. *Science* **2007**, *315*, 954–959.
2. Tsymbal, E. Y.; Kohlstedt, H. Tunneling across a Ferroelectric. *Science* **2006**, *313*, 181–183.
3. Tsymbal, E. Y.; Gruverman, A.; Garcia, V.; Bibes, M.; Barthélémy, A. Ferroelectric and Multiferroic Tunnel Junctions. *MRS Bull.* **2012**, *37*, 138–143.
4. Kohlstedt, H.; Pertsev, N.; Rodríguez Contreras, J.; Waser, R. Theoretical Current-Voltage Characteristics of

Ferroelectric Tunnel Junctions. *Phys. Rev. B* **2005**, *72*, 125341.
5. Zhuravlev, M.; Sabirianov, R.; Jaswal, S.; Tsymbal, E. Giant Electroresistance in Ferroelectric Tunnel Junctions. *Phys. Rev. Lett.* **2005**, *94*, 246802.
6. Garcia, V.; Fusil, S.; Bouzehouane, K.; Enouz-Vedrenne, S.; Mathur, N. D.; Barthélémy, A.; Bibes, M. Giant Tunnel Electroresistance for Non-Destructive Readout of Ferroelectric States. *Nature* **2009**, *460*, 81–84.
7. Gruverman, A.; Wu, D.; Lu, H.; Wang, Y.; Jang, H. W.; Folkman, C. M.; Zhuravlev, M. Y.; Felker, D.; Rzchowski, M.; Eom, C.-B.; *et al*. Tunneling Electroresistance Effect in Ferroelectric Tunnel Junctions at the Nanoscale. *Nano Lett.* **2009**, *9*, 3539–3543.
8. Kim, G.; Mazumdar, D.; Gupta, A. Nanoscale Electroresistance Properties of All-Oxide Magneto-electric Tunnel Junction with Ultra-Thin Barium Titanate Barrier. *Appl. Phys. Lett.* **2013**, *102*, 052908.
9. Chanthbouala, A.; Crassous, A.; Garcia, V.; Bouzehouane, K.; Fusil, S.; Moya, X.; Allibe, J.; Dlubak, B.; Grollier, J.; Xavier, S.; *et al*. Solid-State Memories Based on Ferroelectric Tunnel Junctions. *Nat. Nanotechnol.* **2012**, *7*, 101–104.
10. Gao, X. S.; Liu, J. M.; Au, K.; Dai, J. Y. Nanoscale Ferroelectric Tunnel Junctions Based on Ultrathin $BaTiO_3$ Film and Ag Nanoelectrodes. *Appl. Phys. Lett.* **2012**, *101*, 142905.
11. Yin, Y. W.; Burton, J. D.; Kim, Y.-M.; Borisevich, A. Y.; Pennycook, S. J.; Yang, S. M.; Noh, T. W.; Gruverman, A.; Li, X. G.; Tsymbal, E. Y.; *et al*. Enhanced Tunnelling Electroresistance Effect Due to a Ferroelectrically Induced Phase Transition at a Magnetic Complex Oxide Interface. *Nat. Mater.* **2013**, *12*, 397–402.
12. Zenkevich, A.; Minnekaev, M.; Matveyev, Y.; Lebedinskii, Y.; Bulakh, K.; Chouprik, A.; Baturin, A.; Maksimova, K.; Thiess, S.; Drube, W. Electronic Band Alignment and Electron Transport in Cr/$BaTiO_3$/Pt Ferroelectric Tunnel Junctions. *Appl. Phys. Lett.* **2013**, *102*, 062907.
13. Kim, D. J.; Lu, H.; Ryu, S.; Bark, C.-W.; Eom, C.-B.; Tsymbal, E. Y.; Gruverman, A. Ferroelectric Tunnel Memristor. *Nano Lett.* **2012**, *12*, 5697–5702.
14. Pantel, D.; Goetze, S.; Hesse, D.; Alexe, M. Room-Temperature Ferroelectric Resistive Switching in Ultrathin $Pb(Zr_{0.2}Ti_{0.8})O_3$ Films. *ACS Nano* **2011**, *5*, 6032–6038.
15. Pantel, D.; Goetze, S.; Hesse, D.; Alexe, M. Reversible Electrical Switching of Spin Polarization in Multiferroic Tunnel Junctions. *Nat. Mater.* **2012**, *11*, 289–293.
16. Ricinschi, D.; Yun, K.-Y.; Okuyama, M. A Mechanism for the 150 $\mu C\ cm^{-2}$ Polarization of $BiFeO_3$ Films Based on First-Principles Calculations and New Structural Data. *J. Phys.: Condens. Matter* **2006**, *18*, L97–L105.
17. Ederer, C.; Spaldin, N. Effect of Epitaxial Strain on the Spontaneous Polarization of Thin Film Ferroelectrics. *Phys. Rev. Lett.* **2005**, *95*, 257601.
18. Dupé, B.; Infante, I. C.; Geneste, G.; Janolin, P.-E.; Bibes, M.; Barthélémy, A.; Lisenkov, S.; Bellaiche, L.; Ravy, S.; Dkhil, B. Competing Phases in $BiFeO_3$ Thin Films under Compressive Epitaxial Strain. *Phys. Rev. B* **2010**, *81*, 144128.
19. Hatt, A. J.; Spaldin, N. A. Strain-Induced Isosymmetric Phase Transition in $BiFeO_3$. *Phys. Rev. B* **2010**, *81*, 054109.
20. Béa, H.; Dupé, B.; Fusil, S.; Mattana, R.; Jacquet, E.; Warot-Fonrose, B.; Wilhelm, F.; Rogalev, A.; Petit, S.; Cros, V.; *et al*. Evidence for Room-Temperature Multiferroicity in a Compound with a Giant Axial Ratio. *Phys. Rev. Lett.* **2009**, *102*, 217603.
21. Zhang, J.; He, Q.; Trassin, M.; Luo, W.; Yi, D.; Rossell, M.; Yu, P.; You, L.; Wang, C.; Kuo, C.; *et al*. Microscopic Origin of the Giant Ferroelectric Polarization in Tetragonal-Like $BiFeO_3$. *Phys. Rev. Lett.* **2011**, *107*, 147602.
22. Xiang, P.-H.; Asanuma, S.; Yamada, H.; Inoue, I. H.; Sato, H.; Akoh, H.; Sawa, A.; Ueno, K.; Yuan, H.; Shimotani, H.; *et al*. Strain-Mediated Phase Control and Electrolyte-Gating of Electron-Doped Manganites. *Adv. Mater.* **2011**, *23*, 5822–5827.
23. Gruverman, A.; Rodriguez, B. J.; Dehoff, C.; Waldrep, J. D.; Kingon, A. I.; Nemanich, R. J.; Cross, J. S. Direct Studies of Domain Switching Dynamics in Thin Film Ferroelectric Capacitors. *Appl. Phys. Lett.* **2005**, *87*, 082902.
24. Yang, S. M.; Kim, T. H.; Yoon, J.-G.; Noh, T. W. Nanoscale Observation of Time-Dependent Domain Wall Pinning as the Origin of Polarization Fatigue. *Adv. Funct. Mater.* **2012**, *22*, 2310–2317.
25. Chanthbouala, A.; Garcia, V.; Cherifi, R. O.; Bouzehouane, K.; Fusil, S.; Moya, X.; Xavier, S.; Yamada, H.; Deranlot, C.; Mathur, N. D.; *et al*. A Ferroelectric Memristor. *Nat. Mater.* **2012**, *11*, 860–864.
26. Chua, L. Memristor-The Missing Circuit Element. *IEEE Trans. Circuits Syst.* **1971**, *18*, 507–519.
27. Strukov, D. B.; Snider, G. S.; Stewart, D. R.; Williams, R. S. The Missing Memristor Found. *Nature* **2008**, *453*, 80–83.
28. Seidel, J.; Martin, L. W.; He, Q.; Zhan, Q.; Chu, Y.-H.; Rother, A.; Hawkridge, M. E.; Maksymovych, P.; Yu, P.; Gajek, M.; *et al*. Conduction at Domain Walls in Oxide Multiferroics. *Nat. Mater.* **2009**, *8*, 229–234.
29. Farokhipoor, S.; Noheda, B. Conduction Through 71° Domain Walls in $BiFeO_3$ Thin Films. *Phys. Rev. Lett.* **2011**, *107*, 127601.